

NEAR-INFRARED THERMAL EMISSION FROM WASP-12B: DETECTIONS OF THE SECONDARY ECLIPSE IN Ks, H & J*

BRYCE CROLL¹, DAVID LAFRENIERE², LOIC ALBERT³, RAY JAYAWARDHANA¹, JONATHAN J. FORTNEY⁴, NORMAN MURRAY^{5,6}

Draft version October 19, 2018

ABSTRACT

We present Ks, H & J-band photometry of the very highly irradiated hot Jupiter WASP-12b using the Wide-field Infrared Camera on the Canada-France-Hawaii telescope. Our photometry brackets the secondary eclipse of WASP-12b in the Ks and H-bands, and in J-band starts in mid-eclipse and continues until well after the end of the eclipse. We detect its thermal emission in all three near-infrared bands. Our secondary eclipse depths are $0.309^{+0.013}_{-0.012}\%$ in Ks-band (24σ), $0.176^{+0.016}_{-0.021}\%$ in H-band (9σ) and $0.131^{+0.027}_{-0.029}\%$ in J-band (4σ). All three secondary eclipses are best-fit with a consistent phase, ϕ , that is compatible with a circular orbit: $\phi=0.4998^{+0.0008}_{-0.0007}$. The limits on the eccentricity, e , and argument of periastron, ω , of this planet from our photometry alone are thus $|\cos\omega| < 0.0040$. By combining our secondary eclipse times with others published in the literature, as well as the radial velocity and transit timing data for this system, we show that there is no evidence that WASP-12b is precessing at a detectable rate, and show that its orbital eccentricity is likely zero. Our thermal emission measurements also allow us to constrain the characteristics of the planet's atmosphere; our Ks-band eclipse depth argues strongly in favour of inefficient day to nightside redistribution of heat and a low Bond albedo for this very highly irradiated hot Jupiter. The J and H-band brightness temperatures are slightly cooler than the Ks-band brightness temperature, and thus hint at the possibility of a modest temperature inversion deep in the atmosphere of WASP-12b; the high pressure, deep atmospheric layers probed by our J and H-band observations are likely more homogenized than the higher altitude layer probed by our Ks-band observations. Lastly, our best-fit Ks-band eclipse has a marginally longer duration than would otherwise be expected; this may be tentative evidence for material being tidally stripped from the planet – as was predicted for this system by Li & collaborators, and for which observational confirmation was recently arguably provided by Fossati & collaborators.

Subject headings: planetary systems . stars: individual: WASP-12 . techniques: photometric– eclipses
– infrared: planetary systems

1. INTRODUCTION

Multiwavelength constraints on the thermal emission of hot Jupiters are crucial to precisely defining the spectral energy distributions of these planets and understanding their energy budgets. Interestingly most hot Jupiter thermal emission detections to date have not been at the blackbody peaks of these planets, but at longer wavelengths with the Spitzer Space Telescope ($\lambda > 3 \mu\text{m}$; e.g. Charbonneau et al. 2005; Deming et al. 2005). Probing shorter near-infrared wavelengths at

the blackbody peaks of these planets has only recently been proven feasible first through space-based observations with the Hubble Space Telescope (HST; Swain et al. 2009a), and then from the ground (e.g. de Mooij & Snellen 2009; Sing & Lopez-Morales 2000; Gillon et al. 2009). Our program to detect near-infrared thermal emission from the hottest of the hot Jupiters has also been successful using the Wide-field Infrared Camera (WIRCam) on the Canada-France-Hawaii Telescope (CFHT) to detect the Ks-band thermal emission of TrES-2b (Croll et al. 2010a), TrES-3b including an H-band upper-limit (Croll et al. 2010b), and two eclipses of WASP-3b, including a limit on its temporal variability (Croll et al. in prep.).

In the near-infrared multiple band detections have only been performed on a handful of occasions; such multiple-band detections were performed in narrow wavelength regimes from space via spectroscopy with HST for HD 209458 and HD 189733 (Swain et al. 2009a,b), and arguably recently from the ground for HD 189733 using the Infrared Telescope Facility (Swain et al. 2010), as well as from the ground using the Very Large Telescope in the H & K-bands for the highly irradiated hot Jupiter WASP-19b (Anderson et al. 2010; Gibson et al. 2010). Multiple band detections in the near-infrared are therefore rare compared to the frequent multiple-band detections at longer wavelengths using the IRAC (Fazio et al.

¹ Department of Astronomy and Astrophysics, University of Toronto, 50 St. George Street, Toronto, ON M5S 3H4, Canada; croll@astro.utoronto.ca

² Département de physique, Université de Montréal, C.P. 6128 Succ. Centre-Ville, Montréal, QC, H3C 3J7, Canada

³ Canada-France-Hawaii Telescope Corporation, 65-1238 Malahoa Highway, Kamuela, HI 96743.

⁴ Department of Astronomy and Astrophysics, University of California, Santa Cruz, CA, 95064

⁵ Canadian Institute for Theoretical Astrophysics, 60 St. George Street, University of Toronto, Toronto ON M5S 3H8, Canada

⁶ Canada Research Chair in Astrophysics

* Based on observations obtained with WIRCam, a joint project of CFHT, Taiwan, Korea, Canada, France, at the Canada-France-Hawaii Telescope (CFHT) which is operated by the National Research Council (NRC) of Canada, the Institute National des Sciences de l'Univers of the Centre National de la Recherche Scientifique of France, and the University of Hawaii.

2004), IRS (Houck et al. 2004), or MIPS (Rieke et al. 2004) instruments on the Spitzer Space Telescope. Multiwavelength thermal emission measurements with Spitzer have revealed a wealth of information, including that the most highly irradiated exoplanets seem to harbour hot stratospheres and temperature inversions (Knutson et al. 2008a; Charbonneau et al. 2005; Machalek et al. 2008; Knutson et al. 2008b). One could imagine that obtaining multiwavelength constraints on a planet’s thermal emission in the near-infrared could be equally informative. Furthermore the near-infrared is also an ideal place to directly constrain these planets’ pressure-temperature profiles at depth, dayside bolometric luminosities and the fraction of the incident stellar radiation that is transported from the tidally locked day to nightsides deep in these planets’ atmospheres (Barman 2008).

Here we continue our program using WIRCam on CFHT to detect thermal emission from some of the hottest of the hot Jupiters. Our target was the highly irradiated hot Jupiter WASP-12b. The discovery of the inflated, transiting exoplanet WASP-12b was of immediate interest to those attempting to measure the loss in flux during the secondary eclipses of hot Jupiters in the near-infrared - this was because WASP-12b circles a late F-type star with a period of only ~ 26 hours (Hebb et al. 2009). It is thus exposed to extremely high stellar insolation, with an incident flux of $\sim 9 \times 10^9 \text{ ergs}^{-1} \text{ cm}^{-2}$. The planet is also one of the most inflated hot Jupiters, with a radius of $R_P \sim 1.8 R_J$ and a favourable planet-to-star radius ratio ($R_P/R_* \sim 0.12$; Hebb et al. 2009). It should be heated to an equilibrium temperature of over $\sim 2500 \text{ K}$ assuming isotropic reradiation and a zero Bond albedo⁸. For these reasons it was predicted to display near-infrared thermal emission on the order of 0.1-0.3% of the stellar flux in the J, H & Ks near-infrared bands, assuming isotropic reradiation and a zero Bond albedo. Lopez-Morales et al. (2010) have already reported a detection of the secondary eclipse of WASP-12b in z'-band ($0.9 \mu\text{m}$), and more recently Campo et al. (2010) have presented detections of two eclipses in the four IRAC channels for WASP-12b. Campo et al. (2010), however, did not report the eclipse depths for WASP-12b, and for reasons discussed below the Lopez-Morales et al. (2010) detection has recently been called into question. Thus the atmospheric characteristics of WASP-12b remain largely unconstrained.

In addition to receiving extremely high stellar insolation, WASP-12b is intriguing because the combination of its close proximity to its star and its putative original eccentricity ($e=0.049 \pm 0.015$; Hebb et al. 2009) suggests that it could be precessing at a rate that is detectable with current instruments. Such a putative precession signal was recently claimed by Campo et al. (2010). Although the IRAC eclipses reported by Campo et al. (2010) suggest an $\text{ecos}\omega$ constraint similar to that expected for a circular orbit ($\text{ecos}\omega = -0.0054 \pm 0.0030$), Lopez-Morales et al. (2010) had earlier reported an eclipse detection that was considerably offset from a circular orbit ($|\text{ecos}\omega| = 0.016^{+0.011}_{-0.009}$). While at first glance the two measurements are inconsistent, if the planet pre-

cesses this is not the case. By combining their secondary eclipses with those of Lopez-Morales et al. (2010), together with the original radial velocity data for the system (Hebb et al. 2009), as well as a series of transit-time measurements from the original detection paper and ground-based amateurs (from the Exoplanet Transit Database; Poddany et al. 2010), Campo et al. (2010) show that a precessing orbital model best-fits the data with 2σ confidence. The authors caution that this detection is heavily dependent on the secondary eclipse offset reported by Lopez-Morales et al. (2010). Even more recently, radial velocity observations of WASP-12b have suggested that the eccentricity of WASP-12b is small ($e=0.017^{+0.015}_{-0.010}$; Husnoo et al. 2010) and likely zero, constraining the Campo et al. (2010) precession signal and calling into question the Lopez-Morales et al. (2010) eclipse detection. Nevertheless, the best-fit eccentricity of WASP-12b remains non-zero, and thus this planet could be precessing at a much slower rate than Campo et al. (2010) claim. The definitive nail in the coffin on the claim that WASP-12b is precessing at a detectable rate, will thus only result from further detections of this planet’s secondary eclipse well separated in time from the original eclipse detections.

Also, recently preliminary evidence was presented that material from WASP-12b may be being tidally stripped from the planet and may possibly form a circumstellar disk in this system. Li et al. (2010) predicted this system may have such a disk from material overflowing the Roche lobe of WASP-12b, because WASP-12b’s observed radius in the optical ($R_p \sim 1.79 R_J$; Hebb et al. 2009) is already close to its $2.36 R_J$ Roche lobe radius (as quoted in Fossati et al. 2010a). That WASP-12b may exhibit material overflowing its Roche lobe and a circumstellar disk from this material has recently received possible confirmation from HST Cosmic Origins Spectrograph (COS) observations of this system. From these observations Fossati et al. (2010a) find increased transit depths in the ultraviolet when compared to the optical, indicative of material surrounding WASP-12b overflowing its Roche lobe and blocking out a larger fraction of the stellar flux at these wavelengths. In addition they observe an early ingress of the transit of WASP-12b in their near ultraviolet data; Fossati et al. (2010a) interpret this early ingress as a putative sign of previously stripped material from WASP-12b forming a circumstellar disk. These putative signs of a disk are interesting to observers in the near-infrared, specifically the K-band, as Li et al. (2010) predicted that such a disk in this system may exhibit CO emission as bright as 10 mJy at $2.292 \mu\text{m}$. WASP-12 does not, however, display a significant near-infrared excess (Fossati et al. 2010b).

Here we present detections of WASP-12b’s thermal emission in the Ks (24σ), H (9σ) and J-bands (4σ). Our J-band detection is the first thermal emission measurement in this band. Our photometry favours a circular orbit for WASP-12b ($\text{ecos}\omega = -0.0007^{+0.0013}_{-0.0013}$). By combining our secondary eclipse times with those of Lopez-Morales et al. (2010) and Campo et al. (2010), as well as the radial velocity data of Hebb et al. (2009) and Husnoo et al. (2010), and all the transit-time data for the system, we are able to show that not only is there no evidence to date that WASP-12b is precessing at a

⁸ The Bond albedo is the fraction of the bolometric flux reflected from the planet compared to the incident bolometric radiation.

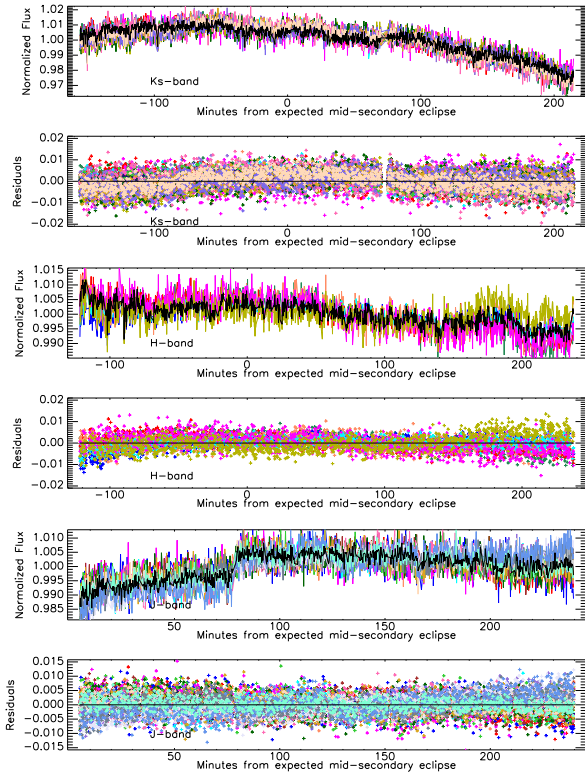


Figure 1. The normalized flux from our target star and reference stars for our Ks-band photometry (top two panels), our H-band photometry (middle two panels), and our J-band photometry (bottom panels). For each set of panels the top panel displays the flux from the target star (black) and the reference stars (various colours) that are used to calibrate the flux of WASP-12b in the various sets of photometry. The bottom panels in each set of panels displays the residuals from the normalized flux of the target star corrected by the normalized flux of the reference stars.

detectable rate, but also that the orbit of WASP-12b is likely circular. Our analysis also allows us to constrain the characteristics of the atmosphere of WASP-12b; our Ks-band eclipse depth argues in favour of inefficient redistribution of heat from the day to nightside, while our J and H-band observations seem to be probing deeper, higher pressure atmospheric layers that are slightly more homogenized. We also show that our Ks-band photometry may feature a longer than expected eclipse duration that could arguably be interpreted as evidence for material streaming from the planet or a circumstellar disk in this system.

2. OBSERVATIONS AND DATA REDUCTION

We obtained observations with WIRCam on CFHT of WASP-12 ($J \sim 10.48$, $H \sim 10.23$, $K \sim 10.19$) on 2009 December 26, 27 and 28 in the J, H & Ks-bands respectively. Our J-band observations on Dec. 26 lasted for 3.9 hours and started in mid-eclipse and persisted for 2.2 hours after the end of eclipse. Our observations on Dec. 27 and 28 lasted for 6.0 hours in H-band and 6.2 hours in Ks-band, respectively, evenly bracketing the predicted secondary eclipse of WASP-12b. Numerous reference stars were also observed in the 21×21 arcmin field-of-view of WIRCam. The telescope was defocused for our various observations to approximately 1.5mm (J-band), 1.8mm (H-band), and 2.0mm (Ks-band), resulting in the flux of our target star being spread over a ring ~ 19 , ~ 23 ,

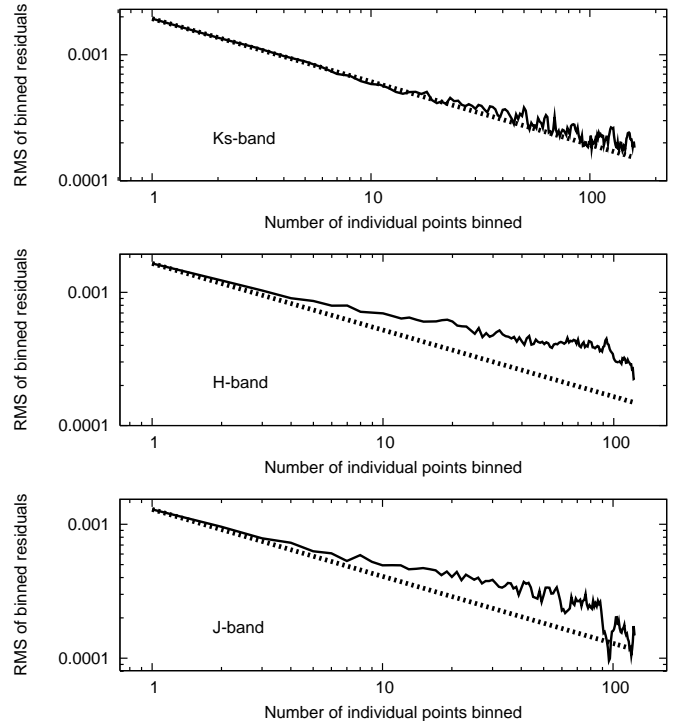


Figure 2. The root-mean-square of our out-of-eclipse photometry (solid line) following the corrections documented in §2 for our Ks-band photometry (top), our H-band photometry (middle), and our J-band photometry (bottom). The dashed line in each panel displays the one over the square-root of the bin-size expectation for gaussian noise.

and ~ 26 pixels in diameter (6, 7 and $8''$) on our array. For each observation, as the telescope temperature changed over the course of the night, we used the focus stage model and kept the defocus amount constant, thus achieved a stable PSF over the entire observation set. We used “Staring Mode” for our J and Ks-band observations where we do not dither for the duration of our observations; for the H-band eclipse the queue observations mistakenly used micro-dithering which featured small 0.5 pixel shifts between consecutive exposures. The exposure times for our J, H & Ks-band observations were 5-seconds. The effective duty cycle after accounting for readout and for saving exposures was 34%.

For both observations the data was reduced and aperture photometry was performed on our target star and our reference stars as discussed in Croll et al. (2010b) (with the details provided in Croll et al. 2010a). We used an aperture with a radius of 17 pixels for our Ks-band photometry, and 16.5 pixels for our H and J-band photometry. We used an annulus to define the sky with an inner radius of 22, and an outer radius of 34 pixels for all our photometry. We ensured that these choices of aperture were optimal by testing smaller and larger aperture sizes in increments of 0.5 pixels and ensuring these choices displayed the smallest root-mean-square (RMS) outside of occultation and the least time-correlated red-noise.

Following our aperture photometry we correct the flux of our target star with a number of nearby reference stars as discussed in Croll et al. (2010a). We used 22, 7, and 17 reference stars to correct our J, H and Ks-band eclipse photometry, respectively. The normalized flux of WASP-

12 and the various reference stars that are used to correct the flux of our target star are displayed in Figure 1. For our Ks-band photometry we corrected our photometry for a small trend with the x , and y pixel position of the target star on the chip⁹. We didn't notice such trends in our H and J-band photometry.

For our H-band photometry the airmass, X , was high at the start of the observations ($X \sim 1.9$), and fell to $X \sim 1.2$ by mid-eclipse. We noticed a downward trend in our H-band photometry following the correction with nearby reference stars that appeared to be correlated with airmass. We found this effect was reduced, but not removed, for our H-band photometry by correcting the flux of WASP-12 with reference stars solely on the same WIRCam chip as WASP-12; this downward trend in flux of our target star compared to the reference stars is still apparent at the start of our H-band photometry. To reduce the impact of these systematic data we scale-up the errors of the first ~ 25 minutes of data for our H-band photometry by a factor of 1.3.

The root-mean-square (RMS) of our photometry per minute following the above corrections improved from 10.0×10^{-3} to 0.86×10^{-3} in Ks-band, 3.8×10^{-3} to 0.90×10^{-3} in H-band and 1.93×10^{-3} to 0.69×10^{-3} in J-band. To evaluate the impact of systematics and the presence of red-noise in our photometry we bin our data and compare the out-of-eclipse photometric precision to the gaussian noise expectation of one over the square-root of the bin-size (Figure 2). The Ks-band data bins down very close to the gaussian noise limit, while the J-band data bins down marginally above this limit; the H-band data is worse, possibly due to the systematics introduced by the micro-dithering. To ensure we do not underestimate the uncertainties in our model parameters we employ the Winn et al. (2008) method to account for time-correlated red-noise in our photometry. We scale-up the uncertainties on our individual data-points by a factor β ; β is equal to the factor that the binned out-of-eclipse RMS scales above the gaussian noise expectation in the absence of red-noise. We use a binning time of ~ 12 minutes. For our H-band photometry we exclude the first 15 minutes of data from this calculation, due to the obvious systematic that we believe to be correlated with airmass that does not appear to affect the rest of the photometry. For our photometry β is equal to 1.7, 1.3 and 1.1 for our J, H & Ks-band data, respectively. We note that our observations are still well above the predicted photon noise RMS limit of 2.7×10^{-4} , 2.2×10^{-4} and 3.1×10^{-4} per minute in the J, H & Ks-bands, respectively.

3. ANALYSIS

For many of our other WIRCam data-sets we have observed residual background trends in the reduced data that seems to affect our target stars differently than our reference stars (Croll et al. 2010a,b, in prep.). For our Ks, H & J-band photometry these backgrounds, B_f , displayed a near-linear slope. We fit our Ks, H & J-band data-sets with linear backgrounds of the form:

$$B_f = 1 + c_1 + c_2 dt \quad (1)$$

⁹ The correction is described in Croll et al. (2010a)

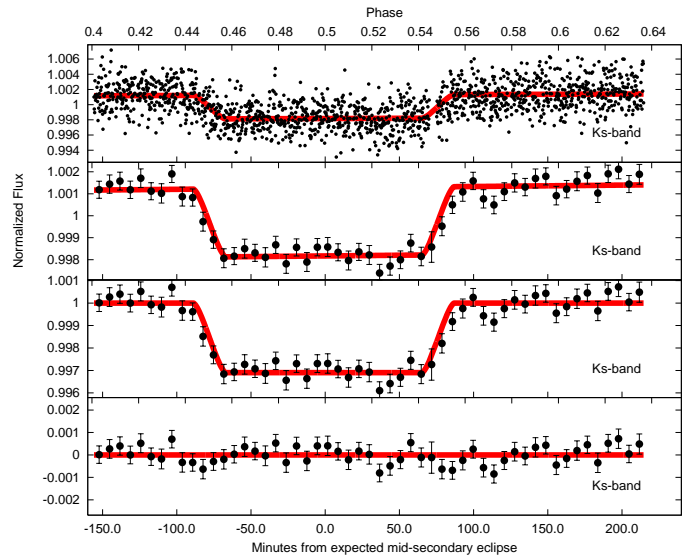


Figure 3. CFHT/WIRCam photometry of the secondary eclipse of WASP-12b observed in the Ks-band on 28 December 2009. The top panel shows the unbinned lightcurve with the best-fit secondary eclipse and background from our MCMC analysis of the Ks-band data with the fixed eclipse duration (red line). The second panel shows the lightcurve with the data binned every ~ 7.0 minutes and again our best-fit eclipse and background. The third panel shows the binned data after the subtraction of the best-fit background, B_f , along with the best-fit eclipse model. The bottom panel shows the binned residuals from the best-fit model.

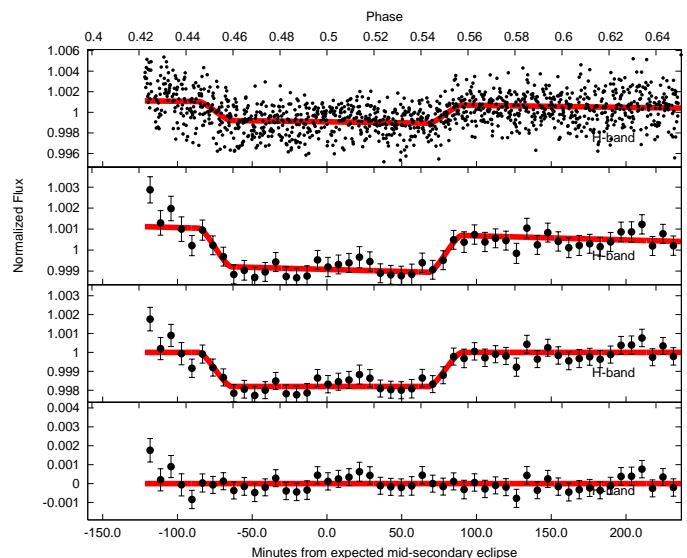


Figure 4. The same as figure 3 except that the data is our H-band photometry obtained on 27 December 2009.

where dt is the interval from the beginning of the observations and c_1 , c_2 and c_3 are fit parameters. We use Markov Chain Monte Carlo (MCMC) fitting to fit for our background as well as a secondary eclipse model calculated from the Mandel & Agol (2002) algorithm without limb darkening. We fit for the background, the depth of the secondary eclipse (ΔF) and the offset that the eclipse occurs later than the expected eclipse center (t_{offset}). Our Markov Chain Monte Carlo method is discussed in Croll (2006) and Croll et al. (2010a). We obtain our stellar and planetary parameters for WASP-

Table 1
Best-fit secondary eclipse parameters

Parameter	Ks-band MCMC Solution	H-band MCMC Solution	J-band MCMC Solution	Joint MCMC Solution	Ks-band MCMC variable eclipse duration solution	Joint MCMC variable eclipse duration solution
reduced χ^2	$0.732^{+0.003}_{-0.001}$	$0.435^{+0.002}_{-0.001}$	$0.358^{+0.003}_{-0.002}$	$0.533^{+0.002}_{-0.001}$	$0.727^{+0.003}_{-0.001}$	$0.532^{+0.001}_{-0.001}$
ΔF_{Ks}	$0.310^{+0.012}_{-0.013}\%$	n/a	n/a	$0.309^{+0.013}_{-0.012}\%$	$0.311^{+0.013}_{-0.011}\%$	$0.313^{+0.011}_{-0.013}\%$
ΔF_H	n/a	$0.180^{+0.015}_{-0.018}\%$	n/a	$0.176^{+0.016}_{-0.021}\%$	n/a	$0.180^{+0.018}_{-0.020}\%$
ΔF_J	n/a	n/a	$0.126^{+0.030}_{-0.013}\%$	$0.131^{+0.027}_{-0.029}\%$	n/a	$0.129^{+0.027}_{-0.031}\%$
t_{offset} (min) ^a	$-1.3^{+1.5}_{-1.2}$	$2.0^{+2.1}_{-2.6}$	$-2.4^{+4.5}_{-4.5}$	$-0.7^{+1.3}_{-1.1}$	$-0.9^{+1.4}_{-1.4}$	$-0.6^{+0.9}_{-1.4}$
$t_{eclipseKs}$ (BJD-2450000)	$5194.9351^{+0.0010}_{-0.0008}$	n/a	n/a	$5194.9356^{+0.0009}_{-0.0007}$	$5194.9355^{+0.0010}_{-0.0010}$	$5194.9356^{+0.0007}_{-0.0010}$
$t_{eclipseH}$ (BJD-2450000)	n/a	$5193.8461^{+0.0014}_{-0.0018}$	n/a	$5193.8441^{+0.0009}_{-0.0007}$	n/a	$5193.8442^{+0.0007}_{-0.0010}$
$t_{eclipseJ}$ (BJD-2450000)	n/a	n/a	$5192.7515^{+0.0031}_{-0.0031}$	$5192.7527^{+0.0009}_{-0.0007}$	n/a	$5192.7528^{+0.0007}_{-0.0010}$
c_{1Ks}	$0.00116^{+0.00014}_{-0.00014}$	n/a	n/a	$0.00116^{+0.00012}_{-0.00015}$	$0.00126^{+0.00016}_{-0.00014}$	$0.00122^{+0.00017}_{-0.00013}$
c_{2Ks} (d^{-1})	$0.001^{+0.001}_{-0.001}$	n/a	n/a	$0.001^{+0.001}_{-0.001}$	$0.001^{+0.001}_{-0.001}$	$0.001^{+0.001}_{-0.001}$
c_{1H}	n/a	$0.00109^{+0.00022}_{-0.00021}$	n/a	$0.00104^{+0.00024}_{-0.00024}$	n/a	$0.00115^{+0.00026}_{-0.00024}$
c_{2H} (d^{-1})	n/a	$-0.003^{+0.001}_{-0.001}$	n/a	$-0.003^{+0.001}_{-0.001}$	n/a	$-0.003^{+0.001}_{-0.001}$
c_{1J}	n/a	n/a	$0.00157^{+0.00027}_{-0.00035}$	$0.00163^{+0.00030}_{-0.00031}$	n/a	$0.00163^{+0.00031}_{-0.00031}$
c_{2J} (d^{-1})	n/a	n/a	$-0.014^{+0.003}_{-0.003}$	$-0.015^{+0.003}_{-0.003}$	n/a	$-0.015^{+0.003}_{-0.003}$
ϕ ^a	$0.4994^{+0.0009}_{-0.0008}$	$0.5015^{+0.0013}_{-0.0017}$	$0.4987^{+0.0028}_{-0.0028}$	$0.4998^{+0.0008}_{-0.0007}$	$0.4997^{+0.0009}_{-0.0009}$	$0.4999^{+0.0006}_{-0.0009}$
$\Phi_{II/I}$	n/a	n/a	n/a	n/a	$1.109^{+0.046}_{-0.039}$	$1.080^{+0.034}_{-0.10}$
Φ_{II} (hours)	2.93	2.93	2.93	2.93	$3.25^{+0.14}_{-0.11}$	$3.16^{+0.10}_{-0.10}$
T_{BKs} (K)	2988^{+45}_{-46}	n/a	n/a	2985^{+49}_{-49}	2993^{+50}_{-51}	3000^{+40}_{-40}
T_{BH} (K)	n/a	2765^{+70}_{-72}	n/a	2748^{+71}_{-74}	n/a	2763^{+80}_{-84}
T_{BJ} (K)	n/a	n/a	2833^{+152}_{-173}	2860^{+138}_{-155}	n/a	2849^{+138}_{-155}
$e \cos(\omega)$ ^a	$-0.0013^{+0.0015}_{-0.0015}$	$0.0020^{+0.0021}_{-0.0021}$	$-0.0024^{+0.0044}_{-0.0044}$	$-0.0007^{+0.0013}_{-0.0013}$	$-0.0009^{+0.0014}_{-0.0014}$	$-0.0006^{+0.0009}_{-0.0009}$
$e \sin(\omega)$	n/a	n/a	n/a	n/a	$0.059^{+0.082}_{-0.034}$	$0.044^{+0.062}_{-0.026}$
f_{Ks}	$0.482^{+0.030}_{-0.029}$	n/a	n/a	$0.480^{+0.032}_{-0.031}$	$0.485^{+0.034}_{-0.033}$	$0.490^{+0.027}_{-0.026}$
f_H	n/a	$0.353^{+0.037}_{-0.036}$	n/a	$0.345^{+0.037}_{-0.036}$	n/a	$0.353^{+0.043}_{-0.041}$
f_J	n/a	n/a	$0.389^{+0.091}_{-0.087}$	$0.405^{+0.085}_{-0.081}$	n/a	$0.399^{+0.083}_{-0.080}$

^a We account for the increased light travel-time in the system (Loeb 2005), and use the best-fit period for the non-precessing case reported by Campo et al. (2010).

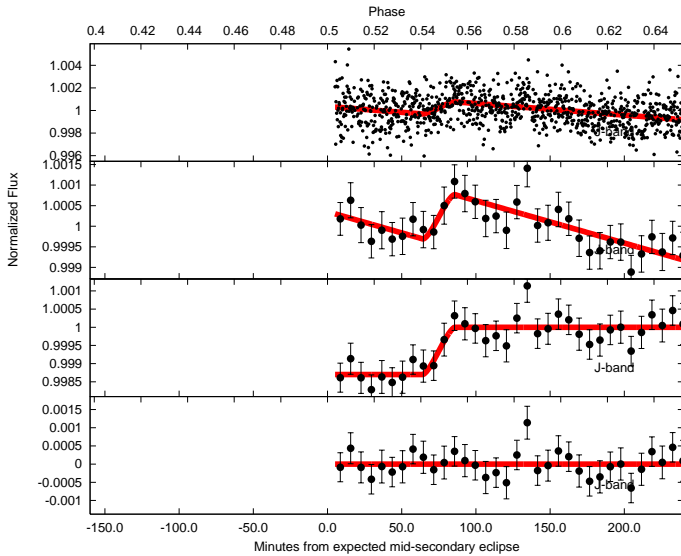


Figure 5. The same as figure 3 except that the data is our J-band photometry obtained on 26 December 2009. Note that the photometry is a partial eclipse only, and starts in eclipse and extends well out of eclipse.

12 from Hebb et al. (2009), while the planetary period and ephemeris are obtained from Campo et al. (2010) from their non-precessing best-fit.

The best-fit secondary eclipses from our individual MCMC analyses with a fixed eclipse duration are presented in Figures 3, 4 and 5 and the best-fit eclipse parameters are presented in Table 1 along with associated parameters, such as the best-fit phase, ϕ , and the barycentric julian date of the eclipse center in the terrestrial time format¹⁰, $t_{eclipse}$. The phase dependence of these fits are presented in Figure 6. We also perform a joint analysis of the three secondary eclipses with a common offset from the eclipse center (t_{offset}); the fit parameters are thus ΔF_{Ks} , ΔF_H , ΔF_J , t_{offset} , and c_1 , and c_2 in each band. The resulting best-fit parameters of this joint fit are listed in Table 1.

We also repeat our fit for our Ks-band photometry, our highest signal-to-noise photometry, and for the joint analysis while fitting for an additional parameter - the duration of the secondary eclipse, Φ_{II} . We parameterize this by the duration of the eclipse divided by the duration of the transit, $\Phi_{II/I}$, using the duration of the transit ($\Phi_I \sim 2.93$ h) reported by Hebb et al. (2009). The results from this fit are presented in Table 1. We do not fit our J-band or H-band data individually with this additional parameter, Φ_{II} , as the J-band data is a partial eclipse and thus the duration of the secondary eclipse is degenerate with an offset of the eclipse center, and the

¹⁰ As calculated using the routines of Eastman et al. (2010).

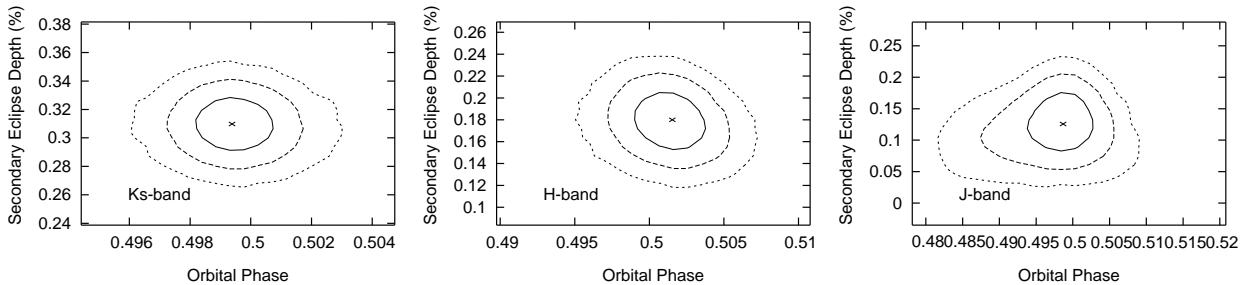


Figure 6. The 68.3% (1σ ; solid-line), 95.5% (2σ ; dashed-line), and 99.7% (3σ ; dotted-line) credible regions from our individual MCMC analyses with a fixed eclipse duration of our Ks-band photometry (left), H-band photometry (middle), and J-band photometry (right). The “x” in the middle of the plots marks the best-fit point from our MCMC analyses.

H-band data suffers from additional time-correlated systematics that could lead to erroneous conclusions.

4. DISCUSSION

We strongly detect all three secondary eclipses in the three near-infrared bands that we observed in. The individual analyses of our three eclipses confirm that all three secondary eclipses are fit with a consistent phase (Table 1); thus the best-fit parameters from our joint analysis are similar to the parameters returned by the analyses of the individual eclipses. We therefore quote the results of the joint analysis below. The best-fit eclipse depths from our joint analysis is $0.309^{+0.013}_{-0.012}\%$ in Ks-band, $0.176^{+0.016}_{-0.021}\%$ in H-band and $0.131^{+0.027}_{-0.029}\%$ in J-band.

4.1. Eccentricity and Precession of WASP-12b

The best-fit phase of the joint analysis is $\phi=0.4998^{+0.0008}_{-0.0007}$. The resulting limit on the eccentricity, e , and argument of periastron, ω , is $ecos\omega=-0.0007^{+0.0013}_{-0.0013}$, a result that is consistent with a circular orbit and the Campo et al. (2010) results. This value is inconsistent, however, with the Lopez-Morales et al. (2010) $ecos\omega$ result. The discrepancy between the Lopez-Morales et al. (2010) result and that of Campo et al. (2010) and our own could be due to WASP-12b precessing - we explore this possibility below.

Campo et al. (2010) performed an analysis of the reported transit times and secondary eclipse times and presented tentative evidence that WASP-12b may be precessing at an observable rate, $\dot{\omega} = 0.02 \pm 0.01^\circ \text{ d}^{-1}$, with a period as short as 40 years. The primary evidence for the precession was the ground-based secondary eclipse detection of Lopez-Morales et al. (2010), which occurred late by approximately ~ 15 minutes (at a phase of $\phi=0.5100^{+0.0072}_{-0.0061}$ using the Hebb et al. 2009 ephemeris and period).

We repeat the Campo et al. (2010) precession analysis adding in our three secondary eclipse detections. We summarize the Campo et al. (2010) precession model that we employ here. The mid-transit time of the N^{th} transit, T_N , in our precessing model is predicted to occur at:

$$T_N = T_o + P_s N - \frac{eP_a}{\pi} (\cos\omega_N - \cos\omega_o). \quad (2)$$

T_o and ω_o are the transit time and argument of periastron at the reference epoch, ω_N is the argument of

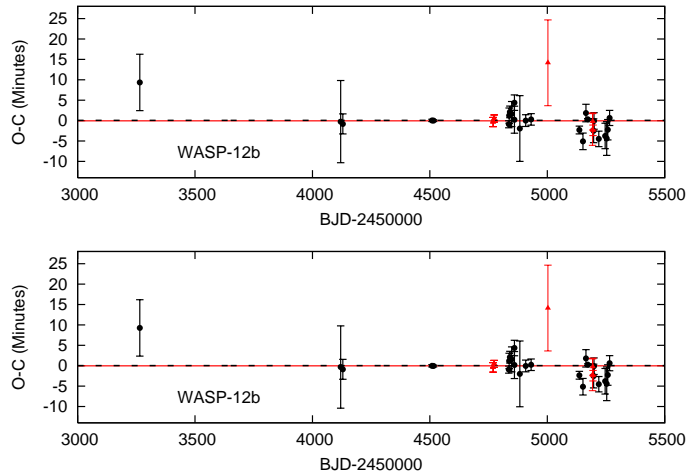


Figure 7. Transit (black points) and eclipse (red points) times for WASP-12b compared to the best-fit orbital models for the precessing case (top), and the non-precessing case (bottom). The best-fit models for the transit times (dotted black line) and the eclipse times (solid red line) are also shown. Both diagrams show the observed-minus-calculated (O-C) times from a linear ephemeris calculated using T_o and P ; the secondary eclipse O-C times are compared to a calculated eclipse centre of $T_o + \frac{P}{2}$. The eclipse points in the two panels are from left-to-right, the Campo et al. (2010) Spitzer/IRAC eclipses (BJD-2450000~4750), the Lopez-Morales et al. (2010) eclipse (BJD-2450000~5000), while the last three red-points are the eclipse times reported here (BJD-2450000~5200).

periastron of the N^{th} transit, P_s is the sidereal period, P_a is the period between successive periastron passages, and e has already been defined as the eccentricity. P_a is not an independent variable, but is related to the sidereal period, P_s , and the constant precession rate, $\dot{\omega}$: $P_a = \frac{P_s}{1 - P_s \frac{\dot{\omega}}{2\pi}}$. The argument of periastron of the N^{th} transit is simply $\omega_N = \dot{\omega}(T_N - T_o) + \omega_o$. Equation 2 is solved iteratively for T_N after it is expanded to fifth order in e (as shown in equation (22) of Ragozzine & Wolf 2009). We fit the radial velocity data from Hebb et al. (2009) and Husnoo et al. (2010)¹¹, and the transits listed in Table 2 of Campo et al. (2010) as well as four additional, recent transits¹²

¹¹ Husnoo et al. (2010) argue that there may be correlated red noise in the Hebb et al. (2009) radial-velocity data, possibly due to a systematic offset in the RV zero-point from night to night. As a result we scale-up the errors for the Hebb et al. (2009) data by a factor of 8 and those of Husnoo et al. (2010) by a factor of 2 to account for possible offsets between these two data-sets. We refer the reader to Husnoo et al. (2010) for further discussion.

¹² The additional transits have mid-transit times

Table 2
WASP-12b orbital parameters

Parameter	Precessing Case	Non-Precessing Case	Non-Precessing Case without the Lopez-Morales et al. (2010) eclipse
P (days)	$1.0914239^{+0.0000004}_{-0.0000004}$	$1.0914238^{+0.0000003}_{-0.0000002}$	$1.0914239^{+0.0000002}_{-0.0000004}$
e	$0.00095^{+0.01365}_{-0.00063}$	$0.00089^{+0.02568}_{-0.00057}$	$0.00087^{+0.02494}_{-0.00058}$
T_o (BJD-2450000)	$4508.9769^{+0.0001}_{-0.0002}$	$4508.9769^{+0.0001}_{-0.0001}$	$4508.9769^{+0.0002}_{-0.0001}$
ω_o ($^\circ$)	$-90.9^{+184.5}_{-4.5}$ a	$-89.9^{+1.8}_{-2.7}$ a	$-90.0^{+180.9}_{-2.7}$ a
$\dot{\omega}$ ($^\circ$ d $^{-1}$)	$0.003^{+0.002}_{-0.001}$	0.0 b	0.0 b
$\text{ecos}\omega_o$	$-0.0000^{+0.0003}_{-0.0008}$	$0.0000^{+0.0004}_{-0.0005}$	$-0.0001^{+0.0005}_{-0.0005}$
$\text{esin}\omega_o$	$-0.004^{+0.016}_{-0.013}$	$-0.015^{+0.015}_{-0.018}$	$-0.015^{+0.017}_{-0.019}$
χ^2	85.5	93.2	91.4
BIC	106.6	110.1	108.2

^a These distributions are bimodal with strong peaks at $\omega \sim 90^\circ$ and -90° (where $\cos\omega \sim 0$).

^b By definition.)

from the Exoplanet Transit database (Poddany et al. 2010) and our own secondary eclipse data along with those of Lopez-Morales et al. (2010), and Campo et al. (2010). We exclude the in-transit radial velocity data as we do not model for the Rossiter-McLaughlin effect (Gaudi & Winn 2007). We follow Campo et al. (2010), and quote the Lopez-Morales et al. (2010) eclipse point that results from the combined photometry from 1.5 eclipses, at a single epoch halfway between their observations (HJD \sim 2455002.8560 \pm 0.0073). T_N of course gives the transit time to compare to the data, we use e , ω_N , T_N and P_a to calculate the eclipse times, and $\omega(t)$ to calculate the radial velocity values. We use the MCMC techniques explained above to calculate the best-fit precessing model, and non-precessing models, except that we fit for $\text{ecos}\omega$ and $\text{esin}\omega$, instead of e and ω , as ω is poorly constrained as the eccentricity approaches zero.

We plot our precessing and non-precessing best-fit models in Figure 7 and present the MCMC results in Table 2. The best-fit models with and without precession are similar. The best-fit precessing model features a very small rate of precession ($\dot{\omega} = 0.003^{+0.002}_{-0.001}$ d $^{-1}$), that barely provides a superior fit once the extra degrees of freedom are taken into account (a Bayesian Information Criterion¹³ of $BIC=106.6$ for the precessing case, compared to $BIC=110.1$ for the non-precessing case). Thus there is not convincing evidence at this date that WASP-12b is precessing.

Given that the timing offset of the Lopez-Morales et al. (2010) eclipse detection may be suspect, we also refit the non-precessing case with this eclipse excluded, and present the MCMC results in Table 2. The distribution of eccentricity values from our MCMC chain without the Lopez-Morales et al. (2010) eclipse is non-gaussian (the bottom left panel of Figure 8) and favours a near-zero eccentricity with a tail to higher eccentricity values; this limit is $e=0.00087^{+0.02494}_{-0.00058}$. This

(HJD) of 2455246.77604 \pm 0.00217 (A. Gibson, TRESCA), 2455253.32414 \pm 0.00287 (F. Lomoz, TRESCA), 2455257.69131 (G. Haagen, TRESCA), and 2455265.33327 \pm 0.00129 (H. Kucakova, TRESCA).

¹³ For the Bayesian Information Criterion (Liddle 2007) lower-values indicate superior fits corrected for the number of free parameters: $BIC=\chi^2 + k\ln N$, where k is the number of free parameters and N is the number of data points.

is due to the fact that although the $\text{ecos}\omega_o$ values for WASP-12b are well-constrained from the radial-velocity data and the combination of the timing of the eclipses and transits (the top-left panel of Figure 8), the $\text{esin}\omega_o$ values are not well-constrained and thus higher eccentricity values are allowed (the top-right panel of Figure 8) for an argument of periastron where $\cos\omega_o \sim 0$ at $\omega_o \sim 90^\circ$ and -90° (as can be seen in the contour plot in the bottom-right panel of Figure 8). Although we are not able to rule out higher eccentricity values for WASP-12b with high confidence, the orbit of WASP-12b is likely circular; thus WASP-12b is no longer an outlier from the expectation of the timescale of tidal circularization for close-in giant exoplanets. The above analysis would be improved by including an a priori constraint on $\text{esin}\omega_o$ using the eclipse duration values from our own eclipses and the Campo et al. (2010) Spitzer/IRAC eclipses. Unfortunately, although Campo et al. (2010) indicate that their best-fit eclipse durations are similar to that of the transits and should thus place a tight constrain on $\text{esin}\omega_o$ near zero, Campo et al. (2010) do not formally fit for the duration of the eclipse and do not include the associated uncertainties. We discuss the implications of fitting our own eclipse durations below.

4.2. A longer duration secondary eclipse; possible signs of material stripped from the planet?

We also fit our Ks-band photometry and our joint J, H & Ks-band photometry with an eclipse model with the eclipse duration as a free parameter. Our best-fit Ks-band variable eclipse duration fit is presented in Figure 9. Our variable eclipse duration fit does argue for a marginally wider secondary eclipse than transit: $\Phi_{II/I} = 1.109^{+0.046}_{-0.039}$, although this result is only significant at the 2.8σ -level. The associated eclipse duration is $\Phi_{II} = 3.25^{+0.14}_{-0.11}$ hours, longer than the ~ 2.93 hour optical transit found by Hebb et al. (2009), and longer than the similar duration IRAC eclipses found by Campo et al. (2010). That the data suggests a wider secondary eclipse than our best-fit model can be seen in the ingress and egress of our Ks-band photometry (Figure 3).

Our joint analysis of our J, H & Ks-band data also argues for a marginally wider secondary eclipse than transit: $\Phi_{II/I} = 1.080^{+0.034}_{-0.034}$, or that the duration of the

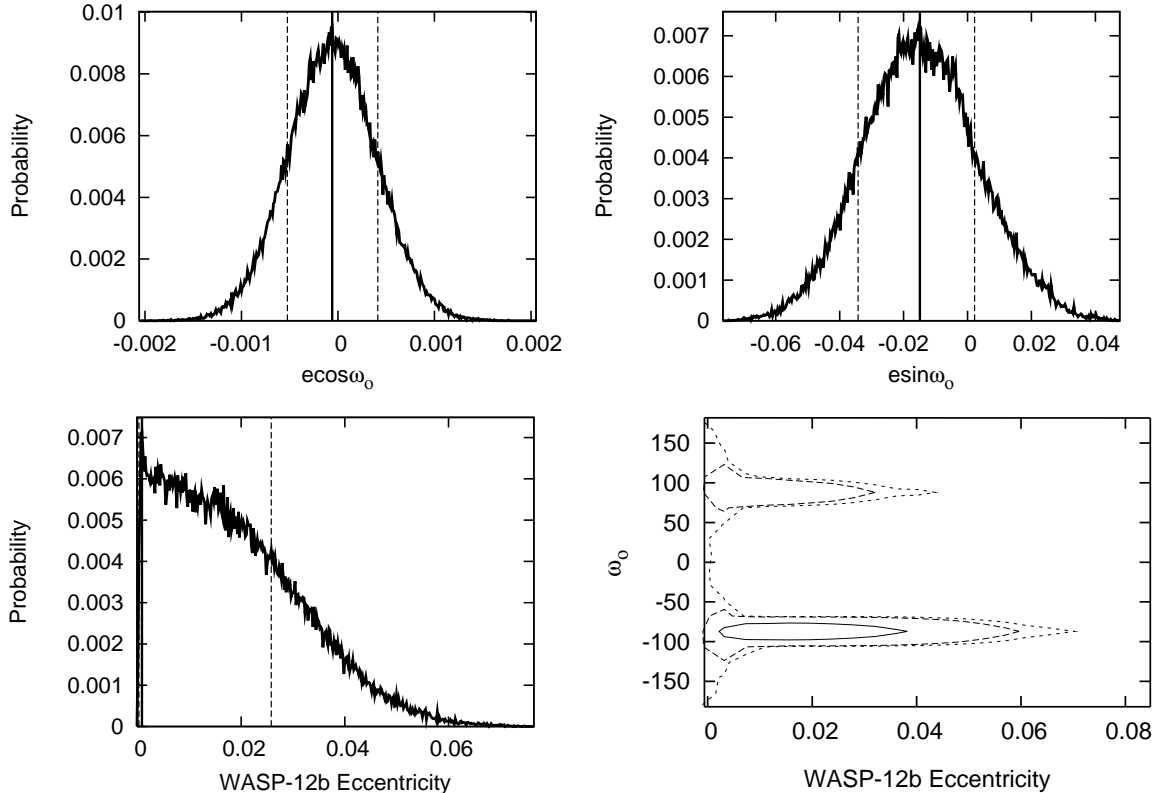


Figure 8. Top-left, top-right and bottom-left panels: Marginalized likelihood for WASP-12b’s $ecos\omega$, $esin\omega$ and its eccentricity from the non-precessing MCMC chain with the Lopez-Morales et al. (2010) point excluded. The best-fit value for each panel is given with the solid vertical line (for the bottom-left panel this value is nearly indistinguishable from zero), while the 68% credible region is indicated by the dotted vertical line. Bottom-right panel: Contour parameter showing the eccentricity, e , and the argument of periastron, ω , of WASP-12b again from the same MCMC chain. The 68.3% (1σ ; solid-line), 95.5% (2σ ; dashed-line), and 99.7% (3σ ; dotted-line) credible regions are indicated.

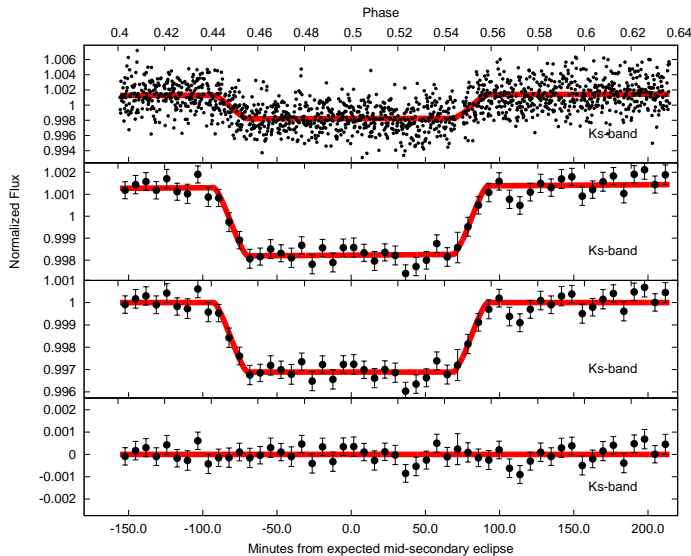


Figure 9. The same as figure 3 except the best-fit model is our variable eclipse duration model for our Ks-band photometry.

eclipse is $\Phi_{II} = 3.16^{+0.10}_{-0.10}$ hours. As our J-band data is a partial eclipse, it has no ability to constrain the eclipse duration on its own. Similarly, as our H-band data suffers from significant systematics prior to and during ingress, its ability to constrain the eclipse duration is compromised; in fact, the systematics at the beginning of the

H-band photometry that manifest themselves as a sharp decrease in flux, can be well-fit by a significantly wider, and deeper secondary eclipse that is unlikely to be physical. These facts, combined with a visual inspection of Figures 3-5, suggests that the wider secondary eclipse for our joint analysis, is in-fact dominated by our Ks-band photometry and the longer duration eclipse may not be credible for the joint analysis.

Our Ks-band photometry is best-fit with a wider secondary eclipse than expected: $\Phi_{II/I} = 1.109^{+0.046}_{-0.039}$. The first possibility to explain this wider than expected eclipse is systematic time-correlated, red-noise in our photometry, which would not be unexpected as the eclipse is only wider than expected at less than the 3σ level. Another possibility for this wider eclipse is that the planet has a small eccentricity ($esin\omega = 0.059^{+0.082}_{-0.034}$). We have already presented strong evidence that the eccentricity of WASP-12b is quite likely near zero in §4.1 and the Campo et al. (2010) Spitzer/IRAC eclipse photometry does not feature a longer duration secondary eclipse. Also, although the $esin\omega$ of the planet is less well constrained in §4.1, an $esin\omega$ value necessary to explain our longer duration eclipse can be ruled out at several sigma and thus we find this possibility unconvincing.

Another possibility – perhaps the most intriguing possibility – is that if this apparently wider secondary eclipse is not due to systematic effects or due to a small $esin\omega$ for WASP-12b, then it could be due to radiation from gas that is escaping from the planet and possibly form-

ing a circumstellar disk. The latter was predicted by Li et al. (2010), while the former was arguably recently confirmed by Fossati et al. (2010a) through observations that WASP-12b displayed increased transit depths in the UV with COS/HST. An eclipse of this duration could argue for material surrounding the planet with a projected radius that is approximately 1.9 times the optical radius of the planet, or at a radius of $3.3 R_{Jupiter}$, and would thus argue for material emitting radiation that is exceeding the Roche lobe, and streaming from the planet. This emission could be due to CO ~ 2.292 bandhead emission, as predicted by Li et al. (2010), although the material around the planet should be cooler than the ~ 4000 - 5000 K temperatures they predicted for the circumstellar disk and will thus result in reduced emission. In the “accretion stream” hypothesis, advocated by (Lai et al. 2010), the material streaming from the planet towards the star may be highly localized in a line passing through the inner Lagrangian point. The extra emission from this stream would be obscured by the star earlier than the planet during eclipse ingress and later than the planet during eclipse egress. Such a scenario is arguably favoured over simply a sphere of evaporating material $3.3 R_{Jupiter}$ in radius, as in the accretion stream scenario the emission will arise from a smaller surface area; otherwise the Ks-band brightness temperature of the planet would have to be anomalously low, given that the $\Delta F_{Ks} = 0.309^{+0.013}_{-0.012}\%$ that we observe would have to be a combination of the planet and the enveloping material that would have a much larger surface area of emitting material than the planet itself.

Alternatively, this wider eclipse could be interpreted as the planet passing behind a circumstellar disk that is optically thick at these wavelengths and extends marginally from the star (at least ~ 1.11 times the stellar radius), and therefore obscures the planet earlier and later than expected. If the disk is optically thick it will have to be due to gas opacity, as the temperature of the disk will be well above the dust sublimation temperature, and the temperature and density of the disk will have to be high enough for the material to be largely photoionized to avoid the “opacity gap” (Thompson et al. 2005). The disk would also have to be optically thick at around $2 \mu m$, but not at the longer wavelengths probed by Spitzer/IRAC (3.6 to $8.0 \mu m$) as the durations of the eclipses are not discrepant from the expected duration in the Campo et al. (2010) photometry. The “accretion stream” hypothesis is arguably less contrived, but the observed eclipse duration could also result from a combination of both scenarios.

An obvious way to differentiate between these two scenarios would be observations of WASP-12 during transit in the Ks-band band. If WASP-12 is surrounded by a circumstellar disk that is emitting in Ks-band then the transit duration will increase. If there is material surrounding WASP-12b then its transit will be of the expected duration if the material is optically thin, and the transit will display an increased depth if the material is optically thick. We plan to perform such follow-up observations of the transit and eclipse of WASP-12b in the Ks and H-bands to differentiate between these various scenarios, and to confirm the near-zero eccentricity of WASP-12b. Until such follow-up observations take place

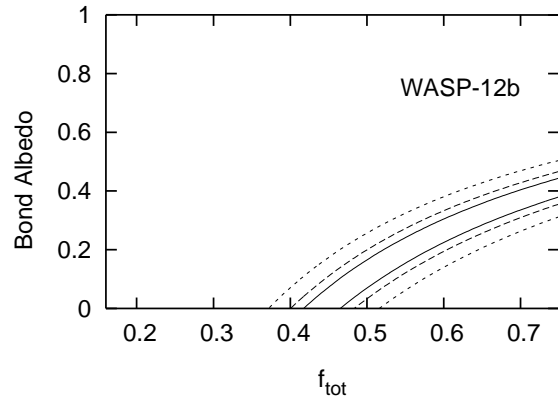


Figure 10. 1σ (solid-lines), 2σ (dashed-lines), and 3σ (dotted-lines) constraints on the Bond albedo and reradiation factor, f_{tot} from our Ks, H & J-band secondary eclipse observations of WASP-12b.

we emphasize that our Ks-band photometry is best-fit with a wider eclipse at less than the 3σ level.

4.3. The properties of WASP-12b’s atmosphere

Our measurements of the thermal emission of WASP-12b allow us to constrain the characteristics of its atmosphere, including: its Bond albedo, the level of redistribution of heat from the day to the nightside at various depths, and the planet’s dayside bolometric luminosity. We parameterize the level of redistribution by the reradiation factor, f , following the Lopez-Morales & Seager (2007) definition (i.e. $f = \frac{1}{4}$ denotes isotropic reradiation, while $f = \frac{1}{2}$ denotes redistribution and reradiation from the dayside only). Our eclipse depths are consistent with a range of Bond albedos, A_B , and overall day to nightside redistribution of heat, f_{tot} (Figure 10). If we assume a Bond albedo near zero, consistent with observations of other hot Jupiters (Charbonneau et al. 1999; Rowe et al. 2008) and with model predictions (Burrows et al. 2008), the best-fit reradiation factor, f_{tot} , that results from our three near-infrared eclipse measurements is $f_{tot} = 0.441^{+0.024}_{-0.023}$. This suggests that the dayside of WASP-12b reradiates most of the incident stellar flux without redistributing it to the nightside.

As the atmospheres of hot Jupiters may be highly vertically stratified, different atmospheric layers may redistribute heat much more or much less efficiently than other layers. The best-fit brightness temperatures and reradiation factors of the individual atmospheric layers probed by our various wavelengths of observations are: $T_{BKs} = 2988^{+45}_{-46} K$ and $f_{Ks} = 0.482^{+0.030}_{-0.029}$ for our Ks-band observations, $T_{BH} = 2765^{+70}_{-72} K$ and $f_H = 0.353^{+0.037}_{-0.036}$ for our H-band observations, $T_{BJ} = 2833^{+152}_{-173} K$ and $f_J = 0.389^{+0.091}_{-0.087}$ for our J-band observations. Our three different bands should be probing high pressure regions, deep into the atmosphere of WASP-12b. Specifically if the near-infrared opacity is dominated by water vapour opacity the J, H & K-bands should be windows in water opacity (Fortney et al. 2008), and the Ks, H & J-bands should be seeing progressively deeper into WASP-12b’s atmosphere. Within the errors the brightness temperatures displayed in our three near-infrared bands are similar. However, the J and H-band brightness temperatures are marginally lower, and taken at face value compared

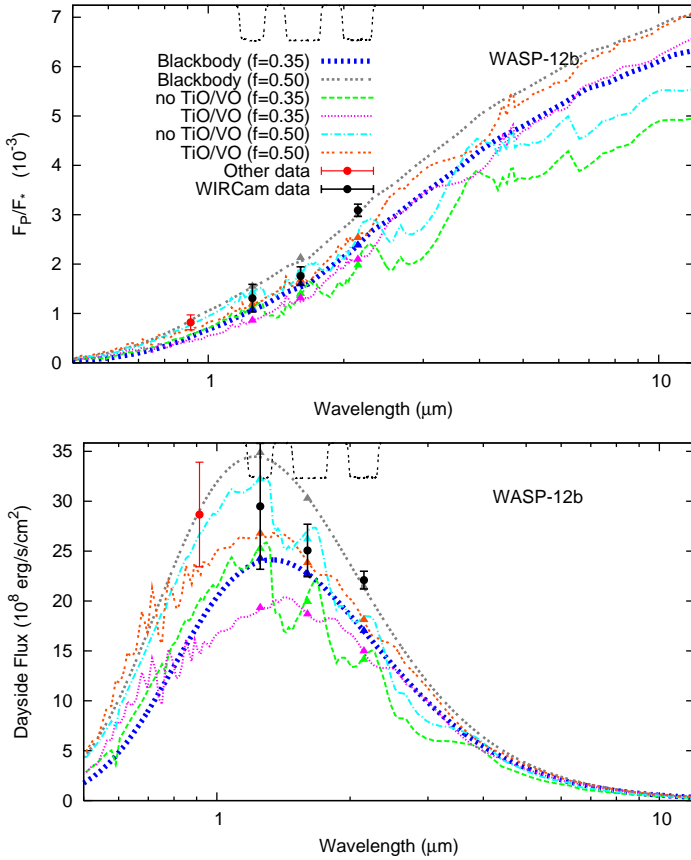


Figure 11. Dayside planet-to-star flux ratios (top) and dayside flux at the planet’s surface (bottom). The Ks-band ($\sim 2.15 \mu\text{m}$), H-band ($\sim 1.60 \mu\text{m}$) and J-band ($\sim 1.25 \mu\text{m}$) points are our own, while the z’-band point ($\sim 0.9 \mu\text{m}$) is from Lopez-Morales et al. (2010). Blackbody curves for modest redistribution ($f=0.35$; $T_{eq}\sim 2735 \text{ K}$; blue dashed line), and dayside only emission ($f=\frac{1}{2}$; $T_{eq}\sim 2990 \text{ K}$; grey dotted line) are also plotted. We also plot one-dimensional, radiative transfer spectral models (Fortney et al. 2006, 2008) for various reradiation factors and with and without TiO/VO. We plot models with modest redistribution ($f=0.35$) with and without TiO/VO (magenta-dotted and green-dashed lines, respectively), and for dayside only emission ($f=\frac{1}{2}$) with and without TiO/VO (orange dotted and cyan dot-dashed lines, respectively). The models with TiO/VO display temperature inversions. The models on the top panel are divided by a stellar atmosphere model (Hauschildt et al. 1999) of WASP-12 using the parameters from (Hebb et al. 2009). ($M_* = 1.35 M_\odot$, $R_* = 1.57 R_\odot$, $T_{eff} = 6300 \text{ K}$, and $\log g = 4.38$). We plot the WIRCam Ks, H and J-band transmission curves inverted at arbitrary scale at the top of both panels (dotted black lines). We integrate our models over the WIRCam bandpasses and display the result in the appropriately coloured triangles.

to the Ks-band brightness temperature they suggest a modest temperature inversion at very high pressures of ~ 100 to 500 mbar, deep in the atmosphere of WASP-12b. One explanation for why WASP-12b might display decreased flux at these shorter wavelengths as compared to the Ks-band, is that the atmospheric depths and pressures probed by these shorter wavelength observations may be more homogenized than higher altitude layers. The efficiency of redistribution of the incident stellar flux from the dayside to the nightside should be proportional to the ratio of the reradiative (τ_{rad}) to advective timescales (τ_{adv}). It is thought that the reradia-

tive timescale should increase with pressure and depth¹⁴. The advective timescale¹⁵ is also thought to increase in pressure, although it is generally thought that advection should win out over reradiation as one descends through the atmosphere of a typical hot Jupiter (Seager et al. 2005; Fortney et al. 2008). Thus, one might expect more efficient redistribution of heat at the layers probed by our shorter wavelength observations compared to the layers probed by our Ks-band observations. Other explanations for the relatively higher Ks-band emission than the H and J-band emission are certainly possible, including: extra flux from a circumstellar disk or material streaming from the planet in the Ks-band, an atmospheric emission feature at Ks-band, or absorption features over the H and J-bands. The eclipse depths from the Campo et al. (2010) Spitzer/IRAC measurements will not shed much additional light on this matter, as, if water opacity dominates, the Spitzer/IRAC bands do not probe as deeply as the JHK near-infrared bands.

We compare the depths of our near-infrared eclipses to a series of planetary atmosphere models in Figure 11. This comparison is made quantitatively as well as qualitatively by integrating the models over the WIRCam J, H & Ks band-passes and calculating the χ^2 of the thermal emission data compared to the models. We include the Lopez-Morales et al. (2010) eclipse depth in Figure 11, but do not include it in our χ^2 calculation due to the aforementioned uncertainty with the timing and depth of this eclipse. The Spitzer/IRAC eclipse depths (Campo et al. 2010) are also not included, as of the time of writing only the central eclipse times have been reported. We first plot two blackbody models, the first one displaying modestly efficient heat redistribution ($f=0.35$; blue dotted line; $T_{eq}\sim 2735 \text{ K}$), while the latter features emission from the dayside only ($f=\frac{1}{2}$; grey dotted line; $T_{eq}\sim 2990 \text{ K}$). The $f=\frac{1}{2}$ blackbody model provides an excellent fit to the longer wavelength Ks-band emission, and does a reasonable job of fitting our H and J-band emission ($f=\frac{1}{2}$; $\chi^2=5$); nevertheless it proves a quantitatively better fit than the modest redistribution model ($f=0.35$; $\chi^2=34$), which generally underpredicts the observed emission.

In Figure 11 we also compare our measurements to a series of one-dimensional, radiative transfer, spectral models (Fortney et al. 2005, 2006, 2008) with different reradiation factors that specifically include or exclude gaseous TiO/VO into the chemical equilibrium and opacity calculations. In these models when TiO/VO are present in gaseous form in the upper atmosphere they act as absorbers at high altitudes and lead to hot stratospheres and temperature inversions (Hubeny et al. 2003). We present models with modest redistribution ($f=0.35$) and dayside only emission

¹⁴ The radiative time-scale (how quickly the planet reradiates the incident stellar flux) is thought to be proportional to $\tau_{rad} \sim \frac{c_P P}{4g\sigma T^3}$ (Showman & Guillot 2002), where c_P is the specific heat capacity, σ is the Stefan-Boltzmann constant, T is the temperature of the atmospheric layer, and g is the gravitational acceleration of the planet.

¹⁵ It is thought that the advective timescale (how quickly the planet advects the heat to the nightside of the planet; τ_{adv}) can be approximated by the radius of the planet, R_P , divided by the horizontal windspeed, U : $\tau_{adv} \sim R_P/U$ (Showman & Guillot 2002).

($f=\frac{1}{2}$) with and without TiO/VO. The associated χ^2 for the $f=\frac{1}{2}$ models with and without TiO/VO are $\chi^2=20$ and $\chi^2=20$, while the $f=0.35$ models with and without TiO/VO are $\chi^2=72$ and $\chi^2=83$. None of these models provide quantitative improvements over the $f=\frac{1}{2}$ blackbody model, as they do not do as good of job of matching the longer wavelength Ks-band thermal emission, nor do they feature reduced emission in H and J-band.

Our near-infrared measurements also allow us to estimate the bolometric dayside luminosity of WASP-12b, L_{day} . We use a blackbody model with a total reradiation factor equal to the best-fit value we calculate from our three near-infrared bands ($f_{tot}=0.441$); by integrating over this model we can estimate L_{day} as $1.12 \times 10^{-3} L_{\odot}$. Another way of parameterizing the efficiency of the day-to-nightside heat redistribution rather than the reradiation factor is comparing the bolometric dayside luminosity, L_{day} , to the nightside luminosity, L_{night} . By following elementary thermal equilibrium calculations one can deduce that WASP-12b should display a total bolometric luminosity of $L_{tot} = 1.25 \times 10^{-3} L_{\odot}$. This suggests that 89% of the incident stellar irradiation is reradiated by the dayside, leaving a mere 11% to be advected to the nightside and reradiated. However, caution is encouraged with this conclusion as shorter and longer wavelength emission for this planet may deviate significantly from that of a blackbody.

4.4. Future Prospects

We lastly note that the combination of thermal emission as prominent as that displayed here with near-infrared photometry this precise suggests the possibility that thermal phase curve measurements may be possible from the ground. For the shortest period exoplanets ($P \sim 1d$ or less) even in a single night of observing (8-9 hours) one could conceivably view the flux maximum of the phase curve where hot gas is advected downwind on the planet, the decrement in flux during the secondary eclipse, and then view a significant fraction of the near-sinusoidal decrease as the cool nightside face of the exoplanet rotates into sight. WASP-12b is an ideal target for such observations with its short 1.09d period, and its bright dayside emission suggests that thermal phase curve observations for this planet should reveal a large asymmetry over the course of the orbit as WASP-12b's nightside should be cold. Thermal phase curve observations from the ground in the near-infrared would require one to control the background systematic trends that are present in our near-infrared photometry even after we correct the flux of our target star with a great many reference stars; the feasibility of this task is, as of yet, unproven. Nevertheless, we will be investigating the possibility of obtaining such near-infrared phase curve information in this photometry as well as with future observations of WASP-12b. These near-infrared phase curve observations will be accompanied by near-simultaneous, 3.6 and 4.5 μm Spitzer/IRAC thermal phase curve observations of a full orbit of WASP-12b (P.I. P. Machalek) that will allow for an unprecedented understanding of the characteristics of the day and nightside deep atmosphere of this planet.

We also plan to reobserve a full, rather than partial, eclipse of WASP-12b in J-band so as to better define

its thermal emission at that wavelength. Lastly we plan to observe the transit of WASP-12b in the near-infrared Ks and H-bands, combined with our aforementioned planned reobservations of the eclipse of WASP-12b in these bands. These combined transit and eclipse observations will allow us to confirm if the Ks-band eclipse is indeed longer in duration than the optical transit, and if so whether this is due to material tidally stripped from the planet that may or may not form a circumstellar disk in this system.

The Natural Sciences and Engineering Research Council of Canada supports the research of B.C. and R.J. The authors thank Daniel Fabrycky, and Darin Ragozzine for helpful discussions on the effects of precession, and Nicolas Cowan for helpful discussions on the putative disk in this system. The authors especially appreciate the hard-work and diligence of the CFHT staff for both scheduling these challenging observations and ensuring these ‘‘Staring Mode’’ observations were successful.

REFERENCES

- Anderson, D.R. 2010, A&A, astro-ph/1002.1947
 Barman, T.S. 2008, ApJ, 676, L61
 Burrows, A. et al. 2008, ApJ, 682, 1277
 Campo, C.J. et al. 2010, astro-ph/1003.2763
 Charbonneau, D. et al. 1999, ApJ, 522, L145
 Charbonneau, D. et al. 2005, ApJ, 626, 523
 Charbonneau, D. et al. 2008, ApJ, 686, 1341
 Croll, B. 2006, PASP, 118, 1351
 Croll, B. et al. 2010a, ApJ, 717, 1084
 Croll, B. et al. 2010b, ApJ, astro-ph/1006-0737
 Croll, B. et al. in preparation
 Deming, D. et al. 2005, Nature, 434, 740
 de Mooij, E.J.W. & Snellen, I.A.G. 2009, A&A, 493, L35
 Eastman, J. et al. 2010, astro-ph/1005.4415
 Fazio, G.G. et al. 2004, ApJS, 154, 10
 Fortney, J.J., et al. 2005, ApJ, 627, L69
 Fortney, J.J., et al. 2006, ApJ, 642, 495
 Fortney, J.J., et al. 2008, ApJ, 678, 1419
 Fossati, L. et al. 2010, ApJ, 714, L222
 Fossati, L. et al. 2010b, astro-ph/1007.3082
 Gaudi, B.S. & Winn, J.N. 2007, ApJ, 655, 550
 Gibson, N.P. 2010, MNRAS, astro-ph/1002.1996
 Gillon, M. et al. 2009, A&A, astro-ph/0905.4571
 Hauschildt, P.H. et al. 1999, ApJ, 512, 377
 Hebb, L. et al. ApJ, 2009, 693, 1920
 Houck, J.R. et al. 2004, ApJS, 154, 18
 Hubeny, I. et al. et al. 2003, ApJ, 594, 1011
 Husnoo, N. et al. et al. 2010, astro-ph/1004.1809
 Knutson, H. et al. 2008a, ApJ, 673, 526
 Knutson, H. et al. 2008b, ApJ, 691, 866
 Lai, D. et al. 2010, astro-ph/1005.4497
 Li, S. et al. 2010, Nature, 463, 1054
 Liddle, A.R. 2007, MNRAS, 377, L74
 Loeb, A. 2005, ApJ, 623, L45
 Lopez-Morales, M. & Seager, S. 2007, ApJ, 667, L191
 Lopez-Morales, M. 2010, astro-ph/0912.2359
 Machalek, P. 2008, ApJ, 684, 1427
 Mandel, K. & Agol, E. 2002, ApJ, 580, L171
 Poddany, S. et al. 2009, New Astronomy, 15, 297
 Ragozzine, D. & Wolf, A.S. 2009, ApJ, 698, 1778
 Rieke, G.H. et al. 2004, ApJS, 154, 25
 Rowe, J. F et al. 2008, ApJ, 689, 1345
 Seager, S. et al. 2005, ApJ, 632, 1122
 Showman, A.P. & Guillot, T. 2002, A&A, 385, 166
 Sing, D.K. & Lopez-Morales, M. 2009, A&A, 493, L31
 Swain, M.R. et al. 2009a, ApJ, 690, L114
 Swain, M.R. et al. 2009b, ApJ, 704, 1616
 Swain, M.R. et al. 2010, Nature, 463, 637

Thompson, T.A. et al. 2005, ApJ, 630, 167
Winn, J. N et al. 2008, ApJ, 683, 1076